RSC Advances

PAPER

View Article Online
View Journal | View Issue

Cite this: *RSC Adv.*, 2018, **8**, 37219

Unbiased spontaneous solar hydrogen production using stable TiO_2–CuO composite nanofiber photocatalysts†

Menna M. Hasan and Nageh K. Allam *

We report on the optimization of electrospun TiO_2–CuO composite nanofibers as low-cost and stable photocatalysts for visible-light photocatalytic water splitting. The effect of different annealing atmospheres on the crystal structure of the fabricated nanofibers was investigated and correlated to the photocatalytic activity of the material. The presence of CuO resulted in narrowing the bandgap of TiO_2 and shifting the absorption edge into the visible region of the light spectrum. The effect of incorporating CuO within TiO_2 nanofibers on the crystal structure and composition was also investigated using X-ray diffraction (XRD), electron paramagnetic resonance (EPR), and X-ray photoelectron spectroscopy (XPS) techniques. The fabricated TiO_2–CuO composite nanofibers showed 117% enhancement in the amount of hydrogen evolved during the photocatalytic water splitting process compared to pure TiO_2. This enhancement was related to the created shallow defect states that facilitate charge transfer from TiO_2 to CuO and distinct characteristics of the composite nanofibers, such as the high surface area and directional charge transfer. The study showed that Cu is a promising alternative to noble metals as a catalyst in photocatalytic water splitting, with the advantage of being an Earth abundant element and a relatively cheap material.

Received 12th August 2018
Accepted 29th October 2018

DOI: 10.1039/c8ra06763e

rsc.li/rsc-advances

Introduction

Using hydrogen as a fuel has many advantages over hydrocarbon fuels, as it is a clean source of energy and possesses higher heat content than gasoline. Photocatalytic water splitting is one of the approaches that has been heavily investigated since the first report by Honda and Fujishima in 1972 using TiO_2 as a photocatalyst.[1,2] TiO_2 is relatively cheap, stable, and Earth abundant, and its valence and conduction band positions are aligned with the redox potential of water. However, there are some limitations that hinder TiO_2 from being an efficient photocatalyst, such as its wide bandgap (almost 3.2 eV), limiting its absorption to the UV region of the solar spectrum, which is only 3–5% of the solar spectrum. Also, TiO_2 suffers a high rate of recombination of the photogenerated electrons and holes. In this regard, doping with noble metals was shown to be very effective in enhancing the photocatalytic activity of TiO_2. However, noble metals are very expensive and not Earth abundant. Thus, finding alternative cost-effective materials is very crucial.[3] On the other hand, blending TiO_2 with other semiconductors of smaller band gap to extend the absorption to a wider range of the solar spectrum.[4] According to previous studies CuO seems to be a promising candidate due to its narrow bandgap (1.4–1.6 eV).[3] Furthermore, CuO can form a p–n junction with TiO_2, which should be very effective in separating the photogenerated charge carriers due to the built-in electrical potential at the interface. This results in the injection of the photogenerated electrons from the CB of TiO_2 to the CB of CuO, which possess more positive potential, while holes accumulate in the VB.[5] Previous studies have shown that incorporating CuO as a co-catalyst with TiO_2 can greatly enhance the efficiency of photocatalytic water splitting. Bandara *et al.* fabricated TiO_2/CuO catalyst, which showed very high catalytic activity, due to the accumulation of the excited electrons from both CuO and TiO_2 in the conduction band of CuO, thus the Fermi level of CuO was shifted upwards, giving the overvoltage needed for water splitting.[6] TiO_2 nanotubes decorated with CuO were fabricated by Xu *et al.*, exhibiting hydrogen rates of around 64.2–71.6 mmol h^{-1} g^{-1}.[7] However, the limited photostability of copper oxides limits their use as a co-catalyst in photocatalytic reactions.[8] The amount of hydrogen reported so far is still far below the theoretical limit of photocatalytic water splitting. On the other hand, CuO_x/TiO_2 composite is mostly investigated in the form of nanoparticles, which suffer high recombination rates at the grain boundaries.[3] As an emerging structure, nanofibers have been investigated by Einert *et al.* using fibrous CuO as a photocathode for photocatalytic water splitting. However, the stability of the electrode was still a limiting issue.[9] Also, Hou *et al.* fabricated electrospun TiO_2/

Energy Materials Laboratory, School of Sciences and Engineering, The American University in Cairo, 11835 New Cairo, Egypt. E-mail: nageh.allam@aucegypt.edu

† Electronic supplementary information (ESI) available. See DOI: 10.1039/c8ra06763e

CuO/Cu mesoporous nanofibers combined with a foaming agent.[5] These electrodes exhibited photocatalytic H_2 yield of almost 851.3 μmol g^{-1} h^{-1}. The authors attributed this enhancement to the presence of a heterojunctions at the TiO_2/CuO, and CuO/Cu interfaces, resulting in more efficient charge carriers separation.[5] However, in almost all those studies previously reported in literature, hole scavengers were used, which is always raising a question whether the obtained hydrogen yield is coming from water splitting or the scavenger (usually methanol) decomposition. Also, some studies apply external bias to drive the water oxidation reaction, which decreases the overall efficiency of the process. Therefore, there is an immense need to find the suitable photocatalysts that can split water in scavengers-free electrolytes and without the need for applied bias.

Herein, we report on the optimized fabrication of electrospun TiO_2–CuO composite nanofibers as efficient catalysts for the photocatalytic water splitting in the absence of any scavengers or applied bias. The nanofiber composites were annealed in different atmospheres and the most photoactive crystalline phase was identified. Also, the effect of different CuO loading on the optical and photocatalytic water splitting performance of the materials was demonstrated.

Experimental methods

Chemicals and materials

Titanium isoprorpoxide, copper(II) acetate monohydrate ($C_4H_6CuO_4 \cdot H_2O$), polyvinylpyrrolidone (PVP, $M_w \approx 1\,300\,000$), ethanol absolute, acetic acid. All chemicals were purchased from Alfa Aesar. All chemicals were used directly without further purification.

Fabrication of nanofibers

TiO_2 nanofibers and TiO_2–CuO composite nanofibers were fabricated using the electrospinning technique. For titanium nanofibers, 0.5 g of titanium isopropoxide was added to 4 g of PVP 10% (the PVP solution was made using polyvinylpyrrolidone (PVP) and ethanol absolute as polymer and solvent, respectively), then 1 g acetic acid was added to the solution, finally the solution was stirred for 2 hours. For pure Cu nanofibers, different weights of copper acetate monohydrate (0.05, 0.075, 0.1, and 0.125) were dissolved in 2.5 g of absolute ethanol, after copper acetate was completely dissolved, 0.25 g of PVP and 5 g of acetic acid were added to the solution, the mixture was then stirred until the polymer is completely dissolved. Ti–Cu composite nanofibers were prepared by mixing the two solutions mentioned before with continuous stirring till complete homogeneity. Finally, each of the three solutions was passed through a 16 G stainless steel nozzle. The distance between the syringe tip and the grounded aluminum foil collector was fixed at 15 cm, the voltage used was in the range of 19 to 21 kV, and the feed rate was in the range of 4 to 4.5 ml h^{-1}, at humidity of 30% to 40%. The electrospun nanofibers were then annealed in a Lindberg/Blue M tube furnace in air and oxygen atmospheres at 450 °C (1 °C min^{-1}) for 2 hours. Table 1 summarizes the composition of the fabricated TiO_2 and TiO_2–Cu composite nanofibers annealed in air and oxygen.

Table 1 Coding of the fabricated TiO_2 and TiO_2–CuO composite nanofibers annealed in air and oxygen

Ti (g)	Cu (g)	Annealing atmosphere	Sample ID
0.5	0	O_2	O1
	0.05		O2
	0.075		O3
	0.1		O4
	0.125		O5
	0	Air	A1
	0.05		A2
	0.075		A3
	0.1		A4
	0.125		A5

Characterization

The morphology of the fabricated nanofibers was characterized with Zeiss SEM Ultra 60 field emission scanning electron microscope (FESEM) and high-resolution transmission electron microscope (HRTEM, JOEL JEM-2100). The thermal stability of the fabricated nanofibers was characterized using TGA NETZSCH STA 409 C/CD apparatus under air. The crystal structure was identified using PANalytical X'pert Pro PW3040 MPD X-ray Diffractometer (XRD) using copper CuK_α radiation ($\lambda = 0.15406$ nm) in the range of 5° to 80° at a scan rate (2θ) of 3° s^{-1} and was further confirmed using Raman microscope (Pro Raman-L Analyzer) with an excitation laser beam wavelength of 532 nm. The absorption spectra of the nanofibers were recorded on a Lambda 950 UV/Vis spectrometer, EPR measurements were performed using Bruker EMX 300 EPR spectrometer (Bruker BioSpin GmbH, Silberstreifen 4, Germany). The photocatalytic activity of the fabricated nanofibers was tested in an inner-irradiation quartz annular reactor with a 300 W xenon lamp (CEL, HUL300), a vacuum pump, a gas collection, a recirculation pump, and a water-cooled condenser. 0.1 g of the sample was suspended in 1 M KOH using ultrasonic oscillator. Then the mixture was transferred into the reactor and deaerated by the vacuum pump. The xenon lamp was utilized as a light source, and the cooling water was circulated through a cylindrical Pyrex jacket located around the light source to maintain the reaction temperature. The reactor was sealed with ambient air during irradiation, and the hydrogen evolution was monitored using an online gas chromatograph (GC, 7900) equipped with a Porapak-Q column, high-purity nitrogen carrier, and a thermal conductivity detector (TCD).

Results and discussion

Fig. 1 shows FESEM images of the fabricated nanofibers before and after annealing. The as-electrospun TiO_2 nanofibers were smooth and highly dense with diameters ranging from 1.594 μm to 2.254 μm, Fig. 1a. Upon annealing in air atmosphere, the diameters were reduced to 180 ± 10 nm, see Fig. 1d. While the Cu nanofibers were completely collapsed upon annealing in air (Fig. 1e), the TiO_2–CuO composite nanofibers maintained their

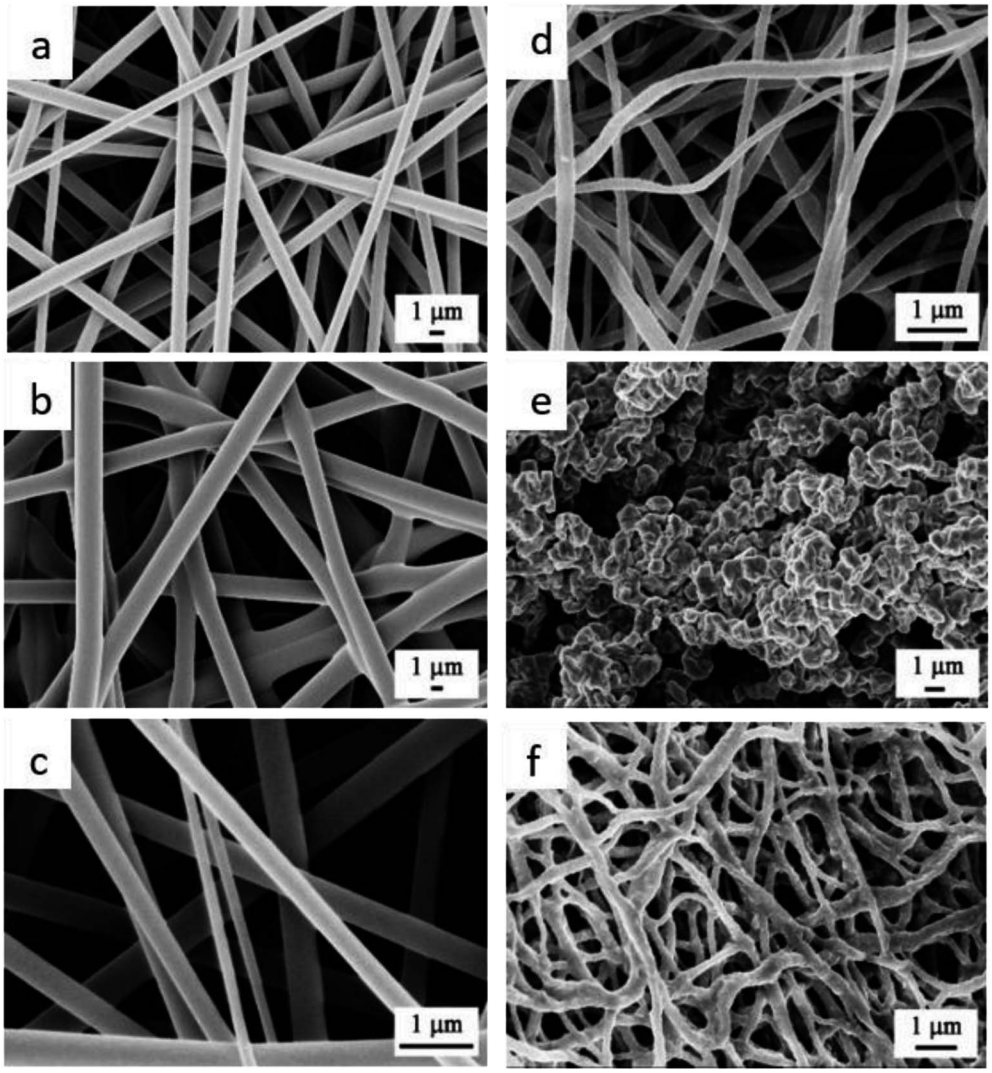

Fig. 1 FESEM images of the electrospun (a) Ti NFs, (b) Cu NFs, (c) Ti–Cu composite NFs before annealing, (d) TiO_2 NFs, (e) CuO NFs, and (f) TiO_2–CuO NFs composite after annealing in air atmosphere.

morphology (Fig. 1f) even with the highest copper concentration, see Fig. S1.† This can be explained by the fact that the crystallization process occurs more rapidly in pure metals than in composites, as in composites, impurity atoms interact with the crystallized grain boundaries and hinder their mobility, leading to a decrease in the crystallization rate. The structural properties of the fabricated NFs were further studied using HRTEM imaging, as shown in Fig. 2. The calculated *d*-spacing was found to be 0.25 nm and 0.35 nm, which are characteristic of the $(\bar{1}11)$ plane of CuO and (101) lattice planes of TiO_2, respectively.[10,11] Comparing the TEM data of TiO_2 NFs and TiO_2–CuO composite NFs annealed in air and oxygen atmospheres, it can be noted that CuO species are well distributed along the nanofibers, forming homogenous composite NFs. This also suggests the formation of heterojunction between TiO_2 and CuO species, which facilitates charge separation and reduces charge recombination.

Fig. 3a shows the TG analyses of the fabricated TiO_2 and TiO_2–CuO composite nanofibers. Four major weight loss steps can be identified in the TG graph of TiO_2 nanofibers. The weight loss (2.78%) below 100 °C can be attributed to the evaporation of the residual moisture or any possible residual traces of the solvent (ethanol). The weight loss between 100 °C and 320 °C (3.11%) can be ascribed to the decomposition of the side chain of PVP. The steep slope in the range 230–470 °C involves a weight loss of 54.52% and can be related to the degradation of the main chain of PVP. The final step involves the conversion of the as-spun titanium oxide nanofibers into the anatase phase.[12–14] In contrary, the TG analysis for the TiO_2–CuO composite nanofibers showed a small weight loss of almost 20% in the temperature range 40–200 °C, which can be related to the evaporation of moisture and any residuals from the solvent. Note the major weight loss (65.5%) in the temperature range 230–370 °C, which can be related to the degradation of the polymer (PVP).[15] No further weight losses were observed up to 800 °C. This is in agreement with the FESEM observations in Fig. 1. Fig. 3b shows the XRD patterns of the fabricated nanofibers annealed under different atmospheres. The XRD pattern

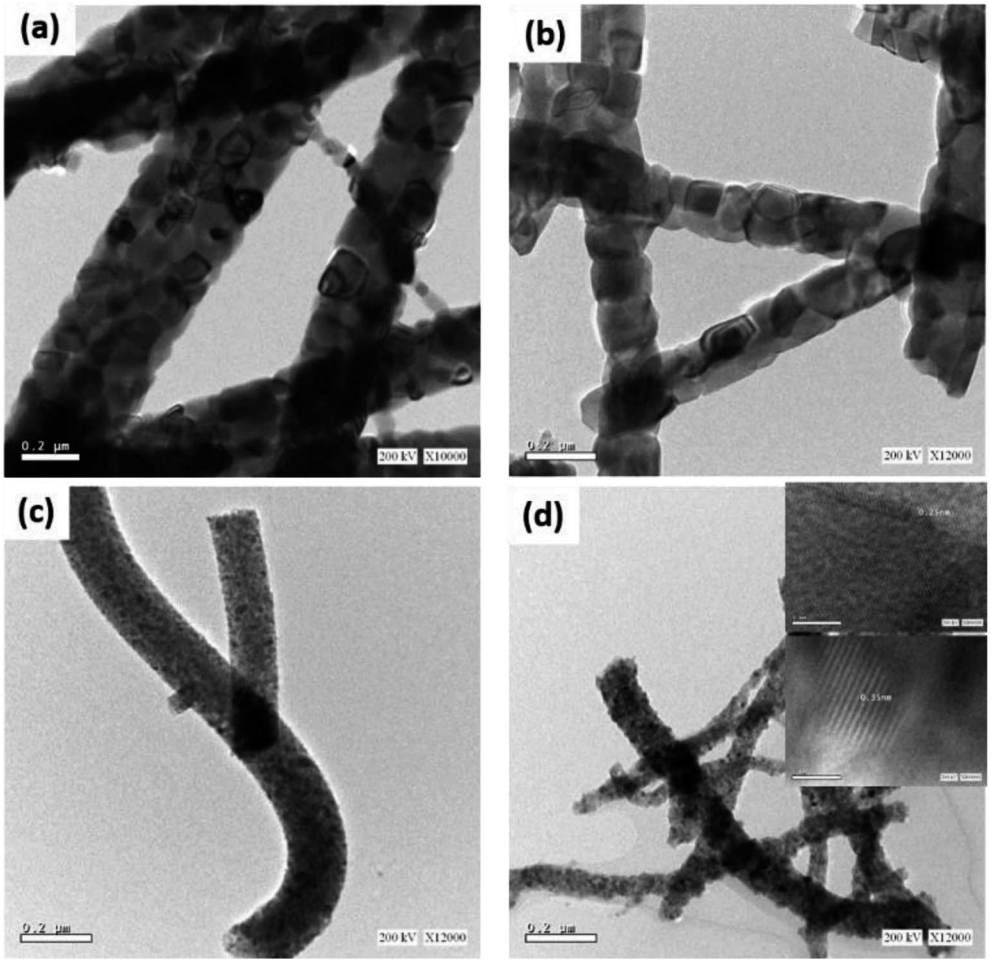

Fig. 2 HRTEM images of (a) TiO_2 NFs and (b) TiO_2–CuO composite NFs annealed in air atmosphere, (c) TiO_2 NFs, and (d) TiO_2–CuO composite NFs annealed in oxygen atmosphere.

of TiO_2 nanofibers annealed in air showed three dominate diffraction peaks at $2\theta = 25.4°$, 37.2° and 48.2°, corresponding to (101), (004), and (200) facets of the anatase phase, respectively.[16,17] However, upon annealing the TiO_2 nanofibers in oxygen, the peaks were observed at $2\theta = 27.4°$, 36°, and 41°, corresponding to (110), (101), and (111) facets of the rutile phase, respectively. In oxygen-rich atmosphere there is a large number of adatoms that react instantly with interstitial Ti^{3+} on the surface forming TiO_x islands, which act as rutile islands, resulting in a very high rate of phase transformation at lower temperature.[18,19] However, in poor-oxygen atmosphere, there is no enough O_2 to react with Ti^{3+}, hindering the phase transformation.[19] This assumption was supported by the electron paramagnetic resonance (EPR) analysis of the sample O1, Fig. S2,† where a weak signal observed at $g = 2.013$, indicating that most of the Ti^{3+} species in the sample were oxidized back to the Ti^{4+} ions. Also, this g value is characteristic of the oxygen radical species $O^{\bullet}$ and O^{2-}.[20–22] For TiO_2–CuO composite nanofibers, the diffraction patterns indicated the formation of the anatase phase in air and rutile phase in oxygen. In both atmospheres, copper was oxidized to CuO as indicated by the presence of new peaks at $2\theta = 35.5°$ and 38.7° corresponding to the $\bar{1}11$, 002 (both appear at the 35.5°), and 111, respectively. For the samples annealed in air atmosphere, after the incorporation of CuO with TiO_2, the diffraction peak at 25.4° became broader and its intensity decreased, indicating a reduction in the crystallite size. This was confirmed by calculating the crystallite size for both samples, which are 318.49 Å and 196.13 Å for A1 and A5, respectively. As Cu^{2+} has larger ionic radius (0.73 Å) than Ti^{4+} (0.64 Å), the incorporated Cu^{2+} ions may distort the lattice structure of TiO_2. This was confirmed by calculating the microstrain, which was found to be 0.551 for A1 and 0.895 for A5. These findings might suggest the creation of substitutional defects by replacing some of the Ti^{4+} ions with Cu^{2+} ions.[23] The formation of oxygen vacancies in the lattice of TiO_2 is also possible to compensate for the charge difference.[23,24] On the other hand, for the oxygen-annealed samples, the broadening of the peak at 27.4° was the same for both TiO_2 and TiO_2–CuO composite nanofibers samples. This might be attributed to the rutile structure being more compact than the anatase phase, requiring more energy to remove the Ti^{4+} ions from the rutile crystal structure and replace it with Cu^{2+} ions.

X-ray photoelectron spectroscopy (XPS) measurements were performed to investigate the chemical environment and electronic structure of Ti, Cu, and O in the fabricated TiO_2–CuO composite nanofibers. Fig. S3† shows the XPS survey for the

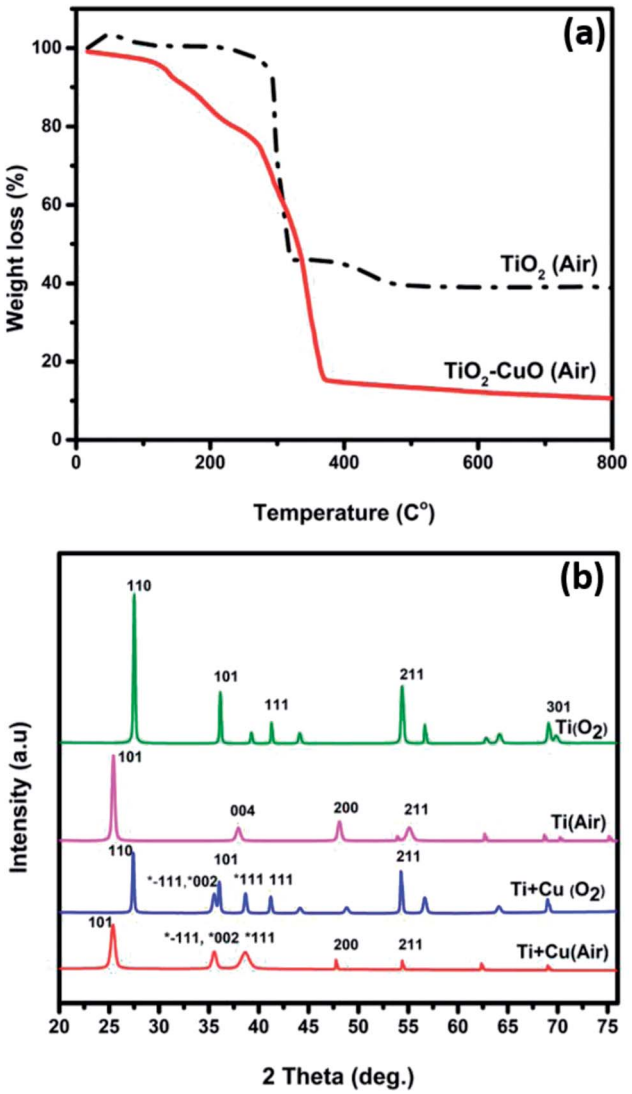

Fig. 3 (a) TG curves of thermal decomposition of as-spun TiO_2 nanofibers in air and (b) XRD pattern of the fabricated nanofibers annealed in different annealing atmospheres.

samples A1 and A4, indicating the presence of titanium, oxygen, copper, and carbon. The HR-XPS scans for Ti, Cu, and O are shown in Fig. 4a–c. The O 1s spectra show a peak at 529.7 eV for both samples. However, for the TiO_2–CuO nanofibers composite, the O 1s peak broadens and two new humps were observed at 531 eV and 528.5 eV, which can be ascribed to Ti^{3+},[25] and oxygen in a defected structure,[26] respectively. Fig. 3c shows two peaks characteristic of Cu^{2+} at 934 and 953 eV related to Cu $2p_{3/2}$ and Cu $2p_{1/2}$.[3,27] A shake-up satellite peak was also observed at 941.28 eV, which is characteristic of CuO species.[28] As shown in Fig. 3b, for both A1 and A4 samples, two peaks were recorded at 458.3 and 463.7 eV related to Ti $2p_{3/2}$ and Ti $2p_{1/2}$, respectively.[29] Upon deconvolution, a small peak was recorded at 456.2, which suggests the formation of Ti^{3+} species[25,30] that have been confirmed *via* EPR analysis.

Electron paramagnetic resonance (EPR) analysis was performed for the sample A1 to confirm the presence of Ti^{3+} species, and the coordination of the Cu^{2+} in the frame work of

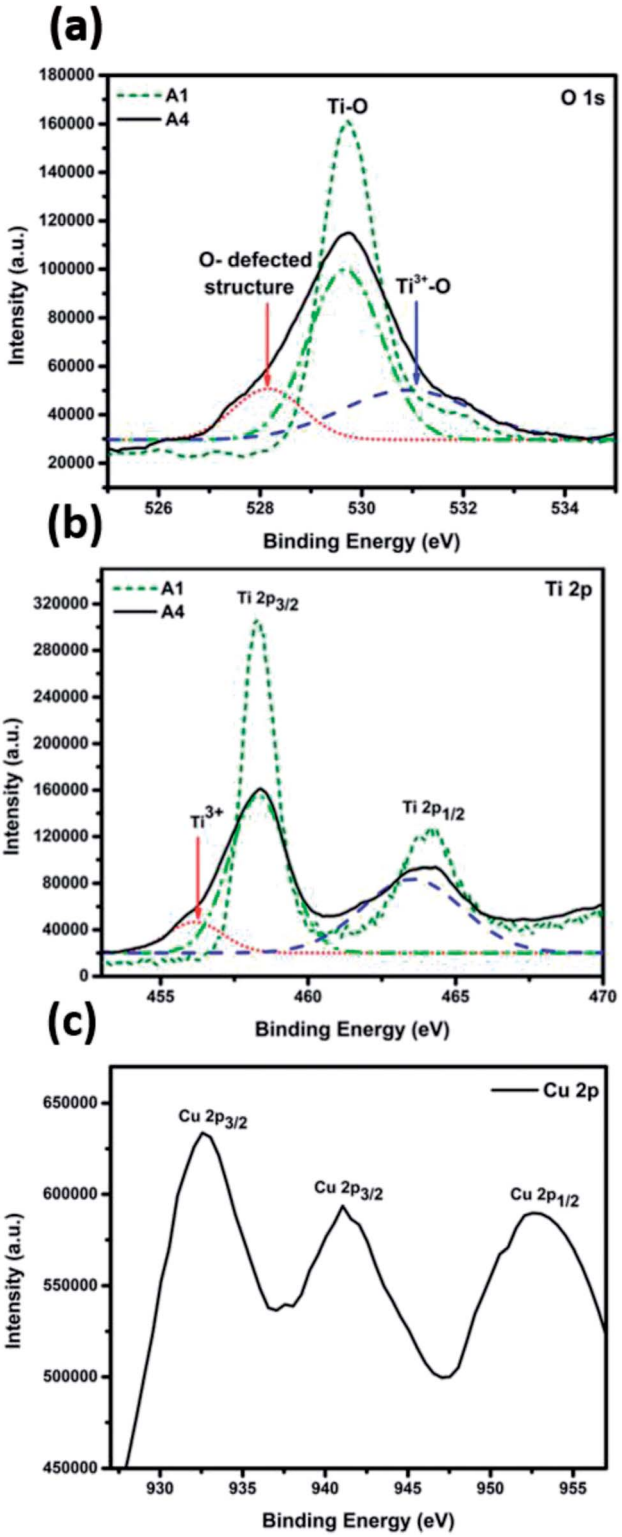

Fig. 4 High resolution XPS spectra of (a) O1s, (b) Ti 2p, and (c) Cu 2p for sample A4.

TiO_2, as shown in Fig. 5a. The EPR signal is asymmetric, indicating the distortion of the octahedral structure, possibly due to the replacement of Ti^{4+} ions with Cu^{2+} in the anatase structure. The EPR spectra show an intense peak at $g_{\parallel} = 2.00072$ and another peak at $g_{\perp} = 2.062$, indicating that Cu^{2+} substituted

Ti^{4+} ions in the octahedral coordination system. As the value of $g_{\perp}$ is larger than that of $g_{\parallel}$, the ground state of the resulting structure is $^2A_{1g}$.[23,24,31,32] The observed peak broadening can be attributed to the dipolar interaction between Cu^{2+} ions.[23]

Fig. 5b shows the Raman spectra of the nanofibers annealed in different atmospheres. The TiO_2 nanofibers annealed in air showed the major four Raman bands of anatase at 158, 410, 524, and 646 cm^{-1}, corresponding to E_g, B_{1g}, A_{1g} and E_g active modes, respectively. On the other hand, the TiO_2 nanofibers annealed in oxygen showed the typical Raman bands of rutile at 163, 265, 445, and 618 cm^{-1}, corresponding to the B_{1g}, two phonon scattering, E_g, and A_{1g} modes, respectively.[17] The Raman spectra was almost the same for the Ti–CuO composite nanofibers with a very small shift, even for the samples containing the highest copper concentration.[16,33] A new peak was observed at 276 cm^{-1} that can be assigned to the A_g mode of CuO.[33] The Ti–O bond lengths (R) were calculated using eqn (1) to be (2 × 1.88, 3 × 2.01 and 2.17 Å) for TiO_2 nanofibers and (2 × 1.9, 3 × 2.15 and 2.4 Å) for TiO_2–CuO composite nanofibers based on the observed Raman bands at 645, 526, and 409 cm^{-1}.

These results prevail that the TiO_6 octahedron in anatase was distorted in case of TiO_2–CuO composite nanofibers.[17]

$$\upsilon_{Ti-O} = 722e^{-1.54946(R\ -\ 1.809)} \quad (1)$$

Fig. 6a shows the UV-Vis absorption spectra of the fabricated nanofibers. The TiO_2 samples annealed in air and oxygen atmospheres exhibited an absorption in the UV region of the light spectrum with a peak at 400 nm and 410, respectively. However, a significant red shift in the absorption spectra was observed for the TiO_2–CuO composite nanofibers. As the concentration of CuO increases, the absorption edge extends to a wider range of the light spectrum, with the sample containing the highest CuO concentration show an extended absorption to the near IR region, corresponding to a bandgap energy of 1.4 eV. Fig. 6b shows the corresponding Tauc plots. Note that as the concentration of CuO increases, the optical band gap decreases from 3 eV for pure TiO_2 to 1.45 eV for the sample with the highest copper concentration (A5). This comes in agreement

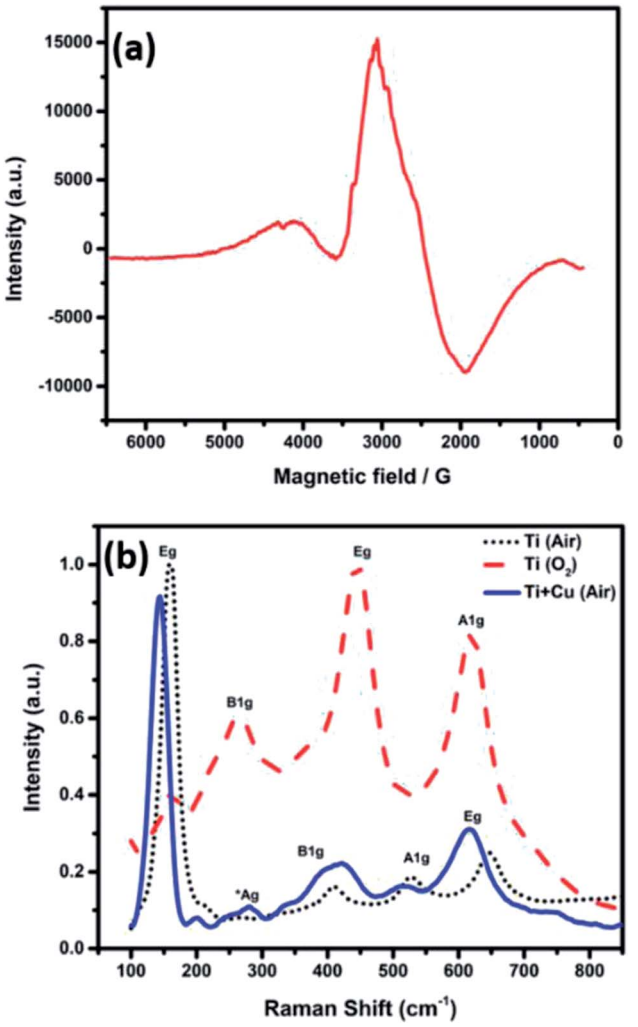

Fig. 5 (a) EPR spectra of TiO_2–CuO composite nanofiber annealed in air and (b) Raman shift of the electrospun nanofibers annealed in different atmospheres.

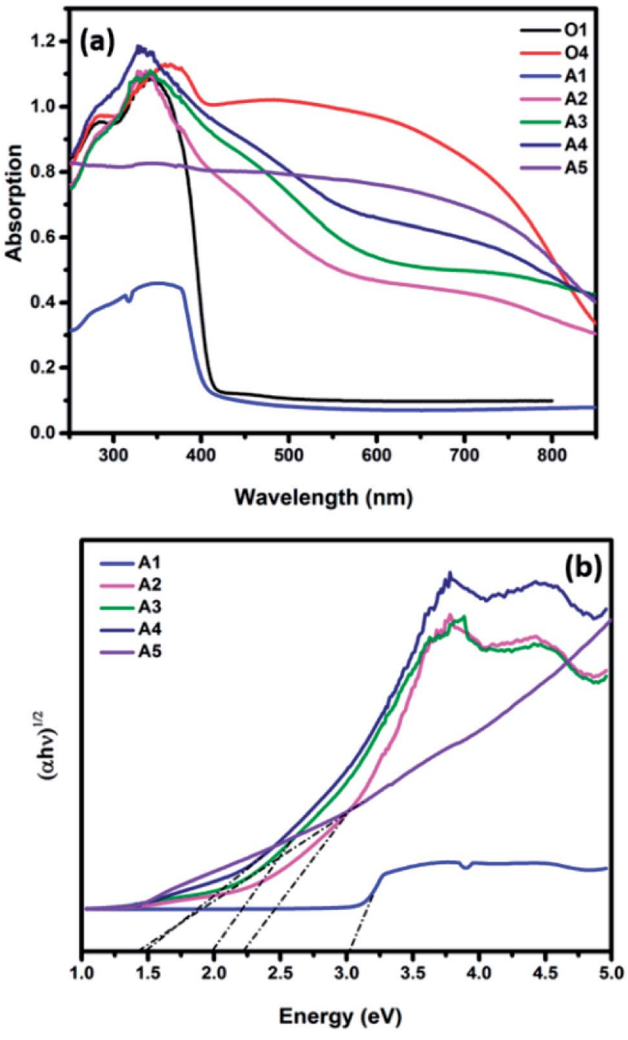

Fig. 6 UV-Visible absorbance spectra of the TiO_2–CuO composite nanofibers with different copper loadings annealed in (a) oxygen and air atmospheres and (b) the corresponding Tauc plots of the air annealed samples.

with the study conducted by Chen *et al.* on the effect of CuO/TiO_2 photocatalyst with different loadings of CuO, where they found that there was a shift in the absorption edge for the CuO/TiO_2 to lower energy as the loading of CuO increased.[34]

The photocatalytic H_2 production activity of the fabricated nanofibers was evaluated under irradiation with a 300 W xenon arc lamp using 1 M KOH solution, Fig. 7. Table 2 summarizes the hydrogen yield obtained upon the use of TiO_2–CuO composites. For TiO_2 nanofibers, the anatase nanofibers showed the highest H_2 yield (1253 μmol g^{-1}), while the rutile nanofibers resulted in lower H_2 yield (919 μmol g^{-1}) due to its band misalignment with the water redox potentials. For both the oxygen- and air-annealed samples, the incorporation of CuO greatly enhances the amount of hydrogen evolved. Fig. 7d shows the normal volcano shape usually seen in catalysis research, where the amount of evolved hydrogen increases with increasing the CuO loading till 0.1 g (1116 and 2715 μmol g^{-1} for the nanofibers annealed in oxygen and air atmospheres, respectively) then declines upon increasing the CuO loading to 0.125 g. This might be attributed to the shielding effect caused by CuO at concentrations higher than 0.1 g, as most of the solar radiation would be absorbed by CuO, thus lower amount of the light is able to reach TiO_2 to excite the electrons in the VB.[24,35] The enhancement in the hydrogen yield can be attributed to the transfer of electrons from the conduction band of TiO_2 to the lower conduction band of CuO,[36–39] due to the formation of a p–n junction between TiO_2 and CuO. This p–n junction is very effective in separating the photogenerated charge carriers and hence enhancing the photocatalytic activity. The hydrogen yield obtained from the fabricated TiO_2–CuO composite nanofibers in absence of a hole scavenger in the electrolyte, is superior compared to previous reports. Recently, CuO_x/TiO_2 composite films were tested for photocatalytic water splitting, with reported hydrogen yield of only 50 mmol m^{-2} h^{-1}.[3] Ternary TiO_2/CuO/Cu mesoporous nanofibers were also tested for photocatalytic water splitting, with the highest hydrogen yield obtained of 851.3 μmol g^{-1} h^{-1}.[5] However, both studies used hole scavenger in the electrolyte to reduce the recombination rate. In this regard, our obtained hydrogen yield, with no hole scavengers, is considered superior, the performance of the fabricated nanofibers in this work is compared with the literature data as shown in Table 3. To test the stability of the fabricated nanofibers, the experiment was repeated for three times. As shown in Fig. 7a and b, the samples showed high stability along 15 hours, then a slight decrease in the hydrogen yield was observed. The structural stability of the fabricated nanofibers was confirmed using FESEM imaging of the materials after the water splitting reaction (irradiation with a 300 W xenon arc lamp using 1 M KOH solution), Fig. S4,† revealing no change in morphology.

To understand the role of individual participating moieties in the catalyst, the photoelectrochemical activity of the fabricated nanofibers to split water was evaluated and discussed in details in the ESI, see Fig. S5.† TiO_2–CuO composite nanofibers annealed in air showed superior photocurrent density than that of TiO_2 nanofibers, indicating the positive effect of CuO when combined with TiO_2 to form a more efficient photocatalyst to split water. The enhanced behavior of TiO_2–CuO composite

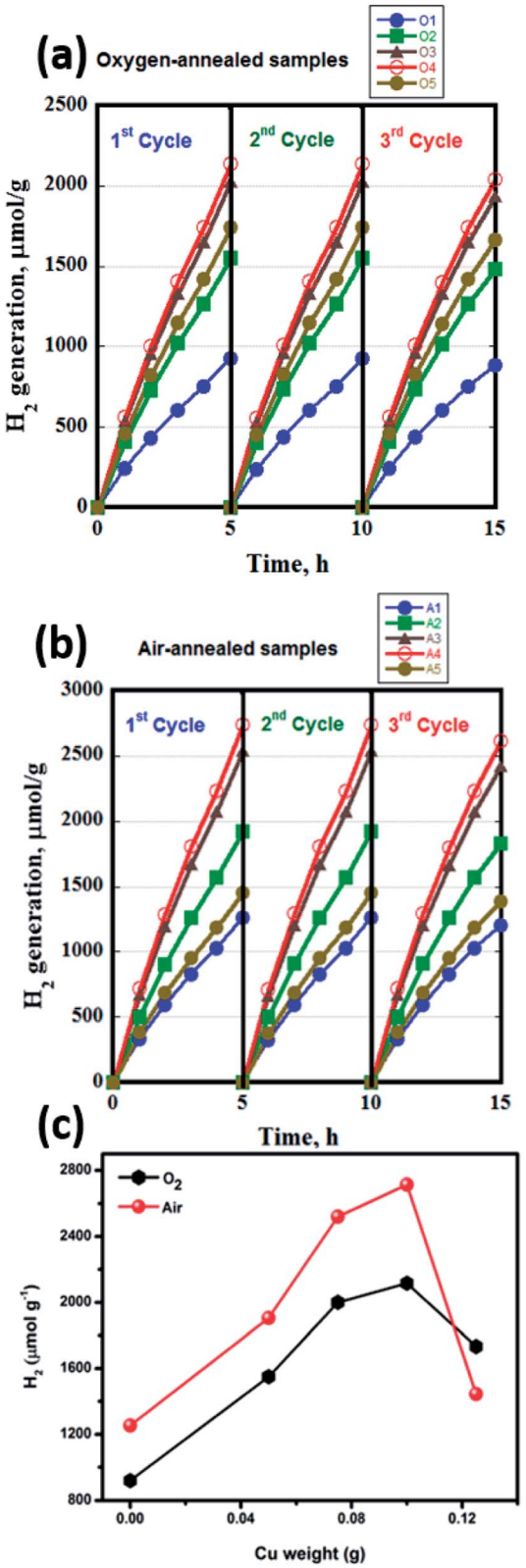

Fig. 7 H_2 evolution measurements for the (a) oxygen annealed samples, (b) the air annealed samples, and (c) the correlation between the H_2 evolution of the different annealing atmospheres and different copper loading.

Table 2 The hydrogen yield obtained upon the use of TiO_2–CuO composite nanofibers annealed in air and oxygen atmospheres

Cu (g)	$[H_2]$ (μmol g^{-1}), (O_2 atmosphere)	$[H_2]$ (μmol g^{-1}), (air atmosphere)
0	919	1253
0.05	1550	1905
0.075	2000	2520
0.1	2116	2715
0.125	1733	1445

Table 3 Comparison of the hydrogen yield obtained in this study with those reported in literature

Photocatalyst	$[H_2]$, μmol g^{-1} h^{-1}	$[H_2]$ mmol m^{-2} h^{-1}
CuO_x/TiO_2 composite films[3]	—	50
Ternary TiO_2/CuO/Cu mesoporous NFs[5]	851.3	—
TiO_2 nanotubes decorated with CuO[7]	64.2–71.6	—
Ti–Cu NFs annealed in oxygen (this work)	2116	—
Ti–Cu NFs annealed in air (this work)	2715	—

nanofibers can be related to the nature of the defects formed due to CuO incorporation.

To understand the role of individual participating moieties in the catalyst, the photoelectrochemical activity of the fabricated nanofibers to split water was evaluated and discussed in details in the ESI, see Fig. S5.† TiO_2–CuO composite nanofibers annealed in air showed superior photocurrent density than that of TiO_2 nanofibers, indicating the positive effect of CuO when combined with TiO_2 to form a more efficient photocatalyst to split water. The enhanced behavior of TiO_2–CuO composite nanofibers can be related to the nature of the defects formed due to CuO incorporation.

Conclusions

In this study, pure TiO_2 and TiO_2–CuO composite nanofibers were fabricated and their structural, thermal, optical and photocatalytic properties were compared. Annealing in different atmospheres was found to determine the crystalline phase and thus photocatalytic activity of the fabricated nanofibers. For the nanofibers crystallized in the anatase phase, XRD and EPR analysis suggest the substitution of some of the Ti^{4+} ions by Cu^{2+} ions, leading to the formation of shallow defect states below the conduction band of TiO_2. Those shallow defects result in a bandgap narrowing and facilitate charge carriers transport and separation. Besides, as the position of the conduction band of CuO is lower than the conduction band of TiO_2, electrons can easily be transferred to CuO, thus enhancing the charge separation process, leaving free charge carriers needed to perform the redox reaction increases. This was supported by measuring the amount of hydrogen evolved, where TiO_2–CuO showed 117% enhancement compared to pure TiO_2 nanofibers. The results of this study prove that manipulating the band structure of TiO_2 using optimized composite formation can be a very promising approach to overcome the limitations of TiO_2 as a photocatalyst for water splitting reaction. It also indicates that copper shows an immense potential as a co-catalyst for photocatalytic water splitting and has a remarkable effect in hindering the recombination of the photogenerated charge carriers, thus enhancing the charge transfer process.

Conflicts of interest

There are no conflicts to declare.

Acknowledgements

The authors acknowledge the financial support of this work by The American University in Cairo. We thank Prof. C. S. Gopinath for the XPS measurements in his laboratory.

Notes and references

1 A. Fujishima and K. Honda, Electrochemical Photolysis of Water at a Semiconductor Electrode, *Nature*, 1972, **238**(5358), 37–38.
2 J. Sundaramurthy, N. Li, P. S. Kumar and S. Ramakrishna, Perspective of Electrospun Nanofibers in Energy and Environment, *Biofuel Res. J.*, 2014, 44–54.
3 Q. Hu, J. Huang, G. Li, J. Chen, Z. Zhang, Z. Deng, Y. Jiang, W. Guo and Y. Cao, Effective Water Splitting Using CuO_x/TiO_2 Composite Films: Role of Cu Species and Content in Hydrogen Generation, *Appl. Surf. Sci.*, 2016, **369**, 201–206.
4 L. Zhu, M. Hong and G. W. Ho, Fabrication of Wheat Grain Textured TiO_2/CuO Composite Nanofibers for Enhanced Solar H_2 Generation and Degradation Performance, *Nano Energy*, 2015, **11**, 28–37.
5 H. Hou, M. Shang, F. Gao, L. Wang, Q. Liu, J. Zheng, Z. Yang and W. Yang, Highly Efficient Photocatalytic Hydrogen Evolution in Ternary Hybrid TiO_2/CuO/Cu Thoroughly Mesoporous Nanofibers, *ACS Appl. Mater. Interfaces*, 2016, **8**(31), 20128–20137.
6 J. Bandara, C. P. K. Udawatta and C. S. K. Rajapakse, Highly Stable CuO Incorporated TiO_2 Catalyst for Photocatalytic

Hydrogen Production from H_2O, *Photochem. Photobiol. Sci.*, 2005, **4**(11), 857.

7 S. Xu, A. J. Du, J. Liu, J. Ng and D. D. Sun, Highly Efficient CuO Incorporated TiO_2 Nanotube Photocatalyst for Hydrogen Production from Water, *Int. J. Hydrogen Energy*, 2011, **36**(11), 6560–6568.

8 M. Janczarek and E. Kowalska, On the Origin of Enhanced Photocatalytic Activity of Copper-Modified Titania in the Oxidative Reaction Systems, *Catalysts*, 2017, **7**(11), 317.

9 M. Einert, T. Weller, T. Leichtweiß, B. M. Smarsly and R. Marschall, Electrospun CuO Nanofibers: Stable Nanostructures for Solar Water Splitting, *ChemPhotoChem*, 2017, **1**(7), 326–340.

10 P. Chandra Rath, J. Patra, D. Saikia, M. Mishra, J.-K. Chang and H.-M. Kao, Highly Enhanced Electrochemical Performance of Ultrafine CuO Nanoparticles Confined in Ordered Mesoporous Carbons as Anode Materials for Sodium-Ion Batteries, *J. Mater. Chem. A*, 2016, **4**(37), 14222–14233.

11 I. Mondal and U. Pal, Synthesis of MOF Templated Cu/CuO@TiO_2 Nanocomposites for Synergistic Hydrogen Production, *Phys. Chem. Chem. Phys.*, 2016, **18**(6), 4780–4788.

12 V. Elayappan, P. Panneerselvam, S. Nemala, K. S. Nallathambi and S. Angaiah, Influence of PVP Template on the Formation of Porous TiO_2 Nanofibers by Electrospinning Technique for Dye-Sensitized Solar Cell, *Appl. Phys. A*, 2015, **120**(3), 1211–1218.

13 W. Nuansing, S. Ninmuang, W. Jarernboon, S. Maensiri and S. Seraphin, Structural Characterization and Morphology of Electrospun TiO_2 nanofibers, *Mater. Sci. Eng., B*, 2006, **131**(1–3), 147–155.

14 M. Hasan, S. Tolba and N. K. Allam, In situ formation of graphene stabilizes the zero-valent copper nanoparticles and significantly enhances the efficiency of photocatalytic water splitting, *ACS Sustainable Chem. Eng.*, DOI: 10.1021/acssuschemeng.8b04219.

15 W. Ponhan and S. Maensiri, Fabrication and Magnetic Properties of Electrospun Copper Ferrite ($CuFe_2O_4$) Nanofibers, *Solid State Sci.*, 2009, **11**(2), 479–484.

16 N. K. Allam, *Anodically fabricated metal oxide nanotube arrays: useful structure for efficient solar energy conversion*, VDM Publishing, 2011.

17 M. Samir, M. Salama and N. K. Allam, Sub-100 Nm TiO_2 Tubular Architectures for Efficient Solar Energy Conversion, *J. Mater. Chem. A*, 2016, **4**(24), 9375–9380.

18 Z. Zhang, J. Lee, J. T. Yates, R. Bechstein, E. Lira, J. Ø. Hansen, S. Wendt and F. Besenbacher, Unraveling the Diffusion of Bulk Ti Interstitials in Rutile TiO_2 (110) by Monitoring Their Reaction with O Adatoms, *J. Phys. Chem. C*, 2010, **114**(7), 3059–3062.

19 M. Wang, J. Wen, Y. Sawada, Y. Hoshi and Z. Hou, Effect of Oxygen and WO_3 Additive on Anatase-to-Rutile Phase Transformation in TiO_2 Nanoparticles, *J. Therm. Anal. Calorim.*, 2015, **119**(1), 435–439.

20 C. Naccache, P. Meriaudeau, M. Che and A. J. Tench, Identification of Oxygen Species Adsorbed on Reduced Titanium Dioxide, *Trans. Faraday Soc.*, 1971, **67**, 506.

21 E. Carter, A. F. Carley and D. M. Murphy, Evidence for O_2 - Radical Stabilization at Surface Oxygen Vacancies on Polycrystalline TiO_2, *J. Phys. Chem. C*, 2007, **111**(28), 10630–10638.

22 J. Strunk, W. C. Vining and A. T. Bell, A Study of Oxygen Vacancy Formation and Annihilation in Submonolayer Coverages of TiO_2 Dispersed on MCM-48, *J. Phys. Chem. C*, 2010, **114**(40), 16937–16945.

23 B. Choudhury, M. Dey and A. Choudhury, Defect Generation, d-d Transition, and Band Gap Reduction in Cu-Doped TiO_2 Nanoparticles, *Int. Nano Lett.*, 2013, **3**(1), 25.

24 G. Li, N. M. Dimitrijevic, L. Chen, T. Rajh and K. a. Gray, Role of Surface/Interfacial Cu^{2+} Sites in the Photocatalytic Activity of Coupled CuO–TiO_2 Nanocomposites, *J. Phys. Chem. C*, 2008, **112**(48), 19040–19044.

25 N. F. Jaafar, A. A. Jalil, S. Triwahyono and N. Shamsuddin, New Insights into Self-Modification of Mesoporous Titania Nanoparticles for Enhanced Photoactivity: Effect of Microwave Power Density on Formation of Oxygen Vacancies and Ti^{3+} Defects, *RSC Adv.*, 2015, **5**(110), 90991–91000.

26 J. Mizera, N. Spiridis, R. P. Socha, M. Zimowska, R. Grabowski, K. Samson and J. Korecki, The Influence of Base Metal (M) Oxidation State in Au-M-O/TiO_2 Systems on Their Catalytic Activity in Carbon Monoxide Oxidation, *Catalysts*, 2011, **2**(4), 38–55.

27 H. Liu, Y. Wang, G. Liu, Y. Ren, N. Zhang, G. Wang and T. Li, An Energy-Efficient Electrochemical Method for CuO – TiO_2 Nanotube Array Preparation with Visible-Light Responses, *Acta Metall. Sin.*, 2014, **27**(1), 149–155.

28 J. Navas, A. Sánchez-Coronilla, T. Aguilar, N. C. Hernández, D. M. de los Santos, J. Sánchez-Márquez, D. Zorrilla, C. Fernández-Lorenzo, R. Alcántara and J. Martín-Calleja, Experimental and Theoretical Study of the Electronic Properties of Cu-Doped Anatase TiO_2, *Phys. Chem. Chem. Phys.*, 2014, **16**(8), 3835.

29 A. Zedan, N. Allam and S. AlQaradawi, A Study of Low-Temperature CO Oxidation over Mesoporous CuO-TiO_2 Nanotube Catalysts, *Catalysts*, 2017, **7**(5), 129.

30 D. Lu, G. Zhang and Z. Wan, Visible-Light-Driven g-C_3N_4/Ti^{3+}-TiO_2 photocatalyst Co-Exposed {0 0 1} and {1 0 1} Facets and Its Enhanced Photocatalytic Activities for Organic Pollutant Degradation and Cr(VI) Reduction, *Appl. Surf. Sci.*, 2015, **358**, 223–230.

31 P. Baltazar, V. H. Lara, G. Córdoba and R. Arroyo, Kinetics of the Amorphous - Anatase Phase Transformation in Copper Doped Titanium Oxide, *J. Sol-Gel Sci. Technol.*, 2006, **37**(2), 129–133.

32 L. Li, X. Shi, C. M. Evans and G. L. Findley, Atomic and Molecular Low-n Rydberg States in Near Critical Point Fluids, in *Advanced Aspects of Spectroscopy*, InTech, 2012.

33 M. R. Pai, A. M. Banerjee, S. A. Rawool, A. Singhal, C. Nayak, S. H. Ehrman, A. K. Tripathi and S. R. Bharadwaj, A Comprehensive Study on Sunlight Driven Photocatalytic Hydrogen Generation Using Low Cost Nanocrystalline Cu-Ti Oxides, *Sol. Energy Mater. Sol. Cells*, 2016, **154**, 104–120.

34 W. T. Chen, V. Jovic, D. Sun-Waterhouse, H. Idriss and G. I. N. Waterhouse, The Role of CuO in Promoting Photocatalytic Hydrogen Production over TiO_2, *Int. J. Hydrogen Energy*, 2013, **38**(35), 15036–15048.

35 S. Slamet, E. Kusrini, A. S. Afrozi and M. Ibadurrohman, Photocatalytic Hydrogen Production from Glycerol-Water over Metal Loaded and Non-Metal Doped Titanium Oxide, *International Journal of Technology*, 2015, **6**(4), 520–532.

36 Z. Jin, X. Zhang, Y. Li, S. Li and G. Lu, 5.1% Apparent Quantum Efficiency for Stable Hydrogen Generation over Eosin-Sensitized CuO/TiO_2 photocatalyst under Visible Light Irradiation, *Catal. Commun.*, 2007, **8**(8), 1267–1273.

37 M. Lei, N. Wang, L. Zhu, Q. Zhou, G. Nie and H. Tang, Photocatalytic Reductive Degradation of Polybrominated Diphenyl Ethers on CuO/TiO_2 nanocomposites: A Mechanism Based on the Switching of Photocatalytic Reduction Potential Being Controlled by the Valence State of Copper, *Appl. Catal., B*, 2016, **182**, 414–423.

38 S. J. A. Moniz and J. Tang, Charge Transfer and Photocatalytic Activity in CuO/TiO_2 Nanoparticle Heterojunctions Synthesised through a Rapid, One-Pot, Microwave Solvothermal Route, *ChemCatChem*, 2015, **7**(11), 1659–1667.

39 N. K. Allam and C. A. Grimes, Electrochemical fabrication of complex copper oxide nanoarchitectures via copper anodization in aqueous and non-aqueous electrolytes, *Mater. Lett.*, 2011, **65**(12), 1949–1955.